

Magnetocaloric effect in the Laves-phase $\text{Ho}_{1-x}\text{Dy}_x\text{Al}_2$ family in high magnetic fields

Bykov, E.; Liu, W.; Skokov, K.; Scheibel, F.; Gutfleisch, O.; Taskaev, S.; Khovaylo, V.; Plakhotskiy, D.; Salazar Mejia, C.; Wosnitza, J.; Gottschall, T.;

Originally published:

September 2021

Physical Review Materials 5(2021), 095405

DOI: <https://doi.org/10.1103/PhysRevMaterials.5.095405>

Perma-Link to Publication Repository of HZDR:

<https://www.hzdr.de/publications/Publ-33218>

Release of the secondary publication
on the basis of the German Copyright Law § 38 Section 4.

Magnetocaloric effect in the Laves-phase $\text{Ho}_{1-x}\text{Dy}_x\text{Al}_2$ family in high magnetic fields

E. Bykov,^{1,2,*} W. Liu,³ K. Skokov,³ F. Scheibel,³ O. Gutfleisch,³ S. Taskaev,^{4,5}
V. Khovaylo,^{5,6} D. Plakhotskiy,⁴ C. Salazar Mejia,¹ J. Wosnitza,^{1,2} and T. Gottschall¹

¹*Dresden High Magnetic Field Laboratory (HLD-EMFL) and Würzburg-Dresden Cluster of Excellence ct.qmat, Helmholtz-Zentrum Dresden-Rossendorf, 01328 Dresden, Germany*

²*Institut für Festkörper- und Materialphysik, Technische Universität Dresden, 01069 Dresden, Germany*

³*Institut für Materialwissenschaft, Technische Universität Darmstadt, Alarich-Weiss-Str. 16, 64287 Darmstadt, Germany*

⁴*Chelyabinsk State University, Br. Kashirinykh Str. 129, 454001 Chelyabinsk, Russia*

⁵*South Ural State University (National Research University), Lenin prospekt 76, 454080 Chelyabinsk, Russia*

⁶*National University of Science and Technology "MISIS", Leninskiy prospect 4, 119991 Moscow, Russia*

(Dated: July 29, 2021)

Hydrogen has the largest gravimetric energy density among all chemical fuels. At the same time, the density of gaseous H_2 is extremely low, which makes its compression to high pressures, liquefaction, or solid-state storage necessary for transport purposes. Liquid hydrogen (LH_2) can be transported in a dewar under atmospheric pressure, but this requires energy-intensive cooling down to 20 K. Magnetocaloric materials have the great potential to revolutionize gas liquefaction in order to make LH_2 more competitive as fuel. In this work, we investigate a series of Laves-phase materials regarding their structural, magnetic, and magnetocaloric properties in high magnetic fields. The three compounds HoAl_2 , $\text{Ho}_{0.5}\text{Dy}_{0.5}\text{Al}_2$, and DyAl_2 are suited for building a stack for cooling from liquid-nitrogen temperature (77 K) down to the boiling point of hydrogen at 20 K. This is evident from our direct measurements of the adiabatic temperature change in pulsed magnetic fields, which we compare with calorimetric data measured in static field. With this methodology, we are now able to study the suitability of magnetocaloric materials down to low temperatures up to the highest magnetic fields.

I. INTRODUCTION

With an ever-increasing energy consumption in the world, modern societies require more and more efficient technologies for energy production and storage. Hydrogen, as a renewable energy carrier, has the highest gravimetric energy density among all chemical fuels of 143 MJ kg^{-1} (lower heating value), which is three times more than for gasoline ($42 - 44 \text{ MJ kg}^{-1}$) or diesel fuel (about 43 MJ kg^{-1}) [1]. Nowadays hydrogen fuel cells demonstrate very high efficiencies between 40 - 60 % [2]. For mobility and storage reasons, also the volumetric energy density has to be taken into consideration. Compressed H_2 at 700 bar possesses only 5.6 MJ L^{-1} [3], which is far less than petrol (32.4 MJ L^{-1}) or diesel (36 MJ L^{-1}) [4]. In liquid form, hydrogen has a volumetric energy density of 10 MJ L^{-1} [5] being still lower than for fossil fuels, but nonetheless relevant for applications. However, the traditional liquefaction of hydrogen is rather inefficient consuming about 40 % of the stored energy content [6]. The development of novel gas-liquefaction techniques can make the production and storage of liquid H_2 more sustainable and competitive compared to other energy carriers.

One of the most perspective alternative approaches is magnetic refrigeration that utilizes the magnetocaloric effect (MCE) of metal compounds [7–9]. This phenomenon describes a change in temperature or entropy of magnetic materials, especially high in the vicinity of their magnetic phase transition temperature, when an external magnetic field is applied [10, 11]. The magnitude of the effect strongly depends on the magnetic properties of the material. Rare-earth compounds are among the most interesting candidates due to their

large magnetic moments caused by the $4f$ electrons [12]. A well-known example is Gd that shows a huge MCE around room temperature [13–17]. However, for the application of the MCE to hydrogen liquefaction, the transition temperature has to be tailored to the desired operational window. In intermetallic compounds, for instance, the interatomic distances and the spin configuration can be tailored leading to the modification of the exchange integral and the Curie temperature, T_C [18]. The transition temperature and, therefore, the maximum position of the MCE can be tuned by the application of external pressure [19–22] or by chemical substitution [23–28]. This variation can then directly be optimized for the operating temperature span for hydrogen liquefaction.

For temperatures below 100 K, Al-based intermetallic binary Laves-phase alloys with rare-earth elements (R) and the general formula $R\text{Al}_2$ show outstanding magnetocaloric effects. These compounds crystallize in the cubic $C15$ MnCu_2 -type structure with space group $Fd\bar{3}m$ [29]. The magnetic properties in $R\text{Al}_2$ are based on the magnetic moments of the rare earths, which order ferromagnetically (FM) below the Curie point. In substituted pseudo-binary Laves-phase alloys, the properties strongly depend on changes in the interatomic distances and the resulting modification of the magnetic interactions [30–36]. De Oliveira *et al.* [35] previously studied the magnetocaloric effect of the $\text{Ho}_{1-x}\text{Dy}_x\text{Al}_2$ system by means of first-principal ab-initio calculations using the Hamiltonian model of interacting $4f$ spins including crystalline electrical field (CEF) effect [37]. Because of the interplay of the different interactions, these alloys have a large magnetic anisotropy. As suggested in [38–40], such compounds can be used in cooling devices based on the anisotropic magnetocaloric effect.

In these compounds, the reported Curie temperatures are found to be in the range from 28 to 42 K for HoAl_2 [37], from

* e.bykov@hzdr.de

58 to 70 K for DyAl₂ [37], and about 43 K for Ho_{0.5}Dy_{0.5}Al₂ [35, 36]. Thus, these three compounds cover the whole temperature region from the liquid-nitrogen boiling point at 77 K down to the hydrogen boiling point at 20 K and can be potentially used for the final stage of hydrogen liquefaction with high performance. In addition, in the ferromagnetic state below T_C a spin-reorientation (SR) transition was observed in HoAl₂ at $T_{SR} \approx 20$ K [36, 41–44], in DyAl₂ at $T_{SR} \approx 40$ K [37, 44, 45] and in Ho_{0.5}Dy_{0.5}Al₂ at $T_{SR} \approx 5$ K [36].

In this work, we provide a comprehensive characterization of the quantities relevant magnetocaloric cooling for HoAl₂, DyAl₂, and Ho_{0.5}Dy_{0.5}Al₂ polycrystals. This includes magnetization, heat capacity, as well as the isothermal entropy and adiabatic temperature change in high magnetic fields.

II. SAMPLE PREPARATION AND METHODS

Polycrystalline samples were synthesized at South Ural State University by arc melting of chemical elements with high purity of 99.998 at.% as described in [46]. For DyAl₂ the synthesis was optimized at the Technical University of Darmstadt in order to reduce the formation of secondary phases, which have a significant influence on the magnetocaloric properties. An excess of amount 3 % Dy was added to the melt.

Powder-diffraction measurements were carried out at room temperature on a X-ray diffractometer using Mo- K_α radiation. The data were evaluated with Rietveld refinement using the FullProf Suite package [47]. Phase-contrast images in the back-scattered electron mode and energy-dispersive X-ray spectroscopy data were obtained using a scanning electron microscope. The specific heat in different magnetic fields was measured in a Physical Properties Measurement System (PPMS) using the 2τ approach between 2 K and room temperature. Magnetization measurements were carried out between 5 and 150 K using PPMS in magnetic fields up to 10 T.

Adiabatic temperature changes ΔT_{ad} were measured directly at the Dresden High Magnetic Field Laboratory of Helmholtz-Zentrum Dresden-Rossendorf in pulsed magnetic fields up to 50 T [17]. The time to reach the maximum field was always 13 ms. Each sample was cut into two flat pieces and a thin type-T thermocouple with a wire thickness of 25 μm was fixed between these pieces by a little amount of silver epoxy. After the samples were fixed on the sample holder, the insert was evacuated to a high vacuum of 10^{-5} mbar. For the sample Ho_{0.5}Dy_{0.5}Al₂ the relative length changes $\Delta l/l_0$ parallel and perpendicular to the applied field direction was studied in pulsed fields simultaneously with ΔT_{ad} by using a two-directional strain gauge sensor, which was glued on the flat sample surface. The sensor resistance was measured using digital lock-in technique described in [48].

III. RESULTS AND DISCUSSION

Figure 1 shows the X-ray diffraction patterns of the Ho_{1-x}Dy_xAl₂ alloys at room temperature and the results of

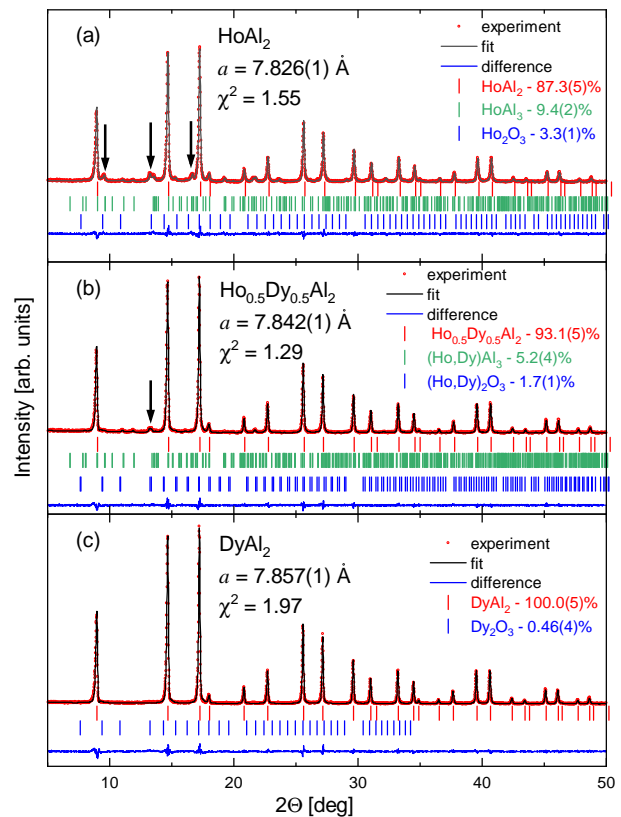


FIG. 1. X-ray diffraction patterns measured at room temperature for Ho_{1-x}Dy_xAl₂ samples with $x = 0, 0.5,$ and 1 (a, b, and c), respectively. Red points correspond to experimental data, black lines stand for calculated patterns, and blue lines for the difference between experimental data and calculation. The vertical bars show the positions of the reflexes from different phases. Black arrows on (a) and (b) show position of reflexes from impurities, which have small intensities compared to the matrix phases and are not described by the $Fd\bar{3}m$ space group.

Rietveld refinement. The small peak width of the reflexes for all samples indicates that the alloys are well crystallized. The HoAl₂, Ho_{0.5}Dy_{0.5}Al₂, and DyAl₂ alloys show multiple phases. The most intensive reflexes are described well by the so-called C15 cubic Laves-phase structure with the space group $Fd\bar{3}m$. The lattice parameters are $a = 7.826(1)$ Å for HoAl₂, $a = 7.842(1)$ Å for Ho_{0.5}Dy_{0.5}Al₂, and $a = 7.857(1)$ Å for DyAl₂ showing a monotonous increase with dysprosium concentration x . The presence of some additional reflexes indicates the existence of secondary phases accounting for about 13 % in total for HoAl₂ (cubic and hexagonal forms of HoAl₃, holmium oxide Ho₂O₃), and about 7 % for Ho_{0.5}Dy_{0.5}Al₂ (cubic and hexagonal forms of HoAl₃ and DyAl₃, as well as holmium and dysprosium oxides). For DyAl₂, the amount of dysprosium oxide is less than 1 %.

We saw further evidence for the presence of secondary phases by electron microscopy (see Fig. 2). Energy-dispersive X-ray spectroscopy analysis shows that besides the matrix phases HoAl₂, Ho_{0.5}Dy_{0.5}Al₂, and DyAl₂ (red arrows in Fig. 2), these samples contain RAl₃ impurities (dark regions,

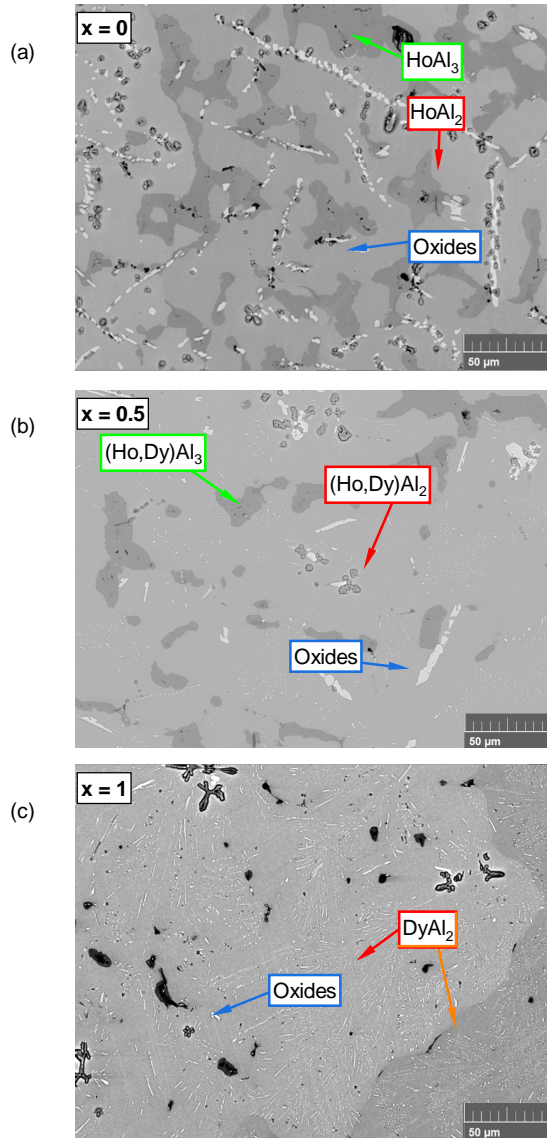


FIG. 2. Backscattered electron images for $\text{Ho}_{1-x}\text{Dy}_x\text{Al}_2$ samples with $x = 0, 0.5, \text{ and } 1$. The different phases are marked by arrows: red and orange for the matrix phase with compositions close to RAl_2 , green for RAl_3 , and blue for oxides. The black spots are pores on the surface of the samples due to polishing.

assigned by green arrows) and small amounts of R_2O_3 oxides (bright areas, blue arrows). The backscattered electron image for DyAl_2 shows two regions with little difference in grey contrast with similar chemical composition ($\text{Dy}_{0.29}\text{Al}_{0.71}$ and $\text{Dy}_{0.28}\text{Al}_{0.72}$, red and orange arrows in Fig. 2(c), respectively). The little white spots are caused by oxides, but the amount is smaller compared to the other two samples. These results are in good agreement with the phase composition from Rietveld refinement. The presence of small black spots can be connected to shadows due to surface topography and little pores or particles on the sample surfaces. Despite the formation of secondary phases, the fraction of the targeted Laves phase is sufficiently high in all samples to study the magnetocaloric

properties. However, we can conclude that the addition of some extra rare earths to the melt formation of secondary phases drastically.

Figures 3(a) and 3(b) show the magnetization M of $\text{Ho}_{1-x}\text{Dy}_x\text{Al}_2$, with $x = 0, 0.5, \text{ and } 1$, as function of temperature and applied magnetic field, respectively. The isofield magnetization data were measured by field cooling regime from 150 K down to 5 K and subsequent heating under applied constant magnetic field between 0.02 T and 10 T in 1 T steps. The data in 0.02 T are plotted using the right-axis scales for better visibility. All curves show a continuous change of the magnetization around the Curie temperatures, typical for a second-order phase transition [49]. T_C shifts towards higher temperatures with increasing Dy concentration, and is 29 K for HoAl_2 , 43 K for $\text{Ho}_{0.5}\text{Dy}_{0.5}\text{Al}_2$, and 62 K for DyAl_2 . These values in agreement with data reported in literature [35–37, 42–45, 50–53]. For the $\text{Ho}_{0.5}\text{Dy}_{0.5}\text{Al}_2$ at 1 T, an additional increase of the magnetization below 10 K is observed [black arrow in Fig. 3(a)], which we relate to the spin-reorientation transition [36].

Using the static magnetic susceptibility $\chi = M/H$ and the Curie-Weiss law, we describe the magnetic behavior above T_C and in low fields by:

$$\chi^{-1} = \frac{T - \theta_p}{C}, \quad (1)$$

where θ_p is the paramagnetic transition temperature and C is the Curie constant. The Curie constant is connected with the effective magnetic moment per rare-earth ion by the relation:

$$\mu_{eff} = \frac{1}{\mu_B} \sqrt{\frac{Cm3k_B}{\rho\mu_0N_A}}, \quad (2)$$

where μ_B is the Bohr magneton, m the molar weight, k_B the Boltzmann constant, ρ the density, μ_0 the permeability of vacuum, and N_A the Avogadro constant. As can be seen exemplarily for HoAl_2 in the inset of Fig. 3(a), the sample follows the Curie-Weiss law and the effective moments per rare-earth ion μ_{eff} extracted from the fits are $10.47 \mu_B$ for $x = 0$, $10.42 \mu_B$ for $x = 0.5$ and $11.0 \mu_B$ for $x = 1$, which are a bit different than the theoretical values ($10.7 \mu_B$ for $x = 0$ [54] and $10.1 \mu_B$ for $x = 1$ [55]).

The field dependences of M , measured in external magnetic fields up to 10 T at different temperatures with 5 K steps around T_C , are plotted in Fig. 3(b). The magnetization at lowest temperatures exceeds $200 \text{ A m}^2 \text{ kg}^{-1}$ for all three compounds and is not fully saturated even at 10 T, as can be seen in Fig. 3(b).

On the basis of the magnetization data in Fig. 3(b), we want to study the universal behavior further. First, we corrected the data for demagnetizing effects. The internal field is derived from $H_i = H_{ext} - NM$, where N is the demagnetization factor $N = 1/\chi_{max}$, that can be approximated by χ_{max} , the maximum slope value of the isothermal magnetization curves in low fields [56]. **The resulting N values vary for the three samples pieces that we used for magnetization measurements due to their slightly different shapes. N is equal to about 0.17 for**

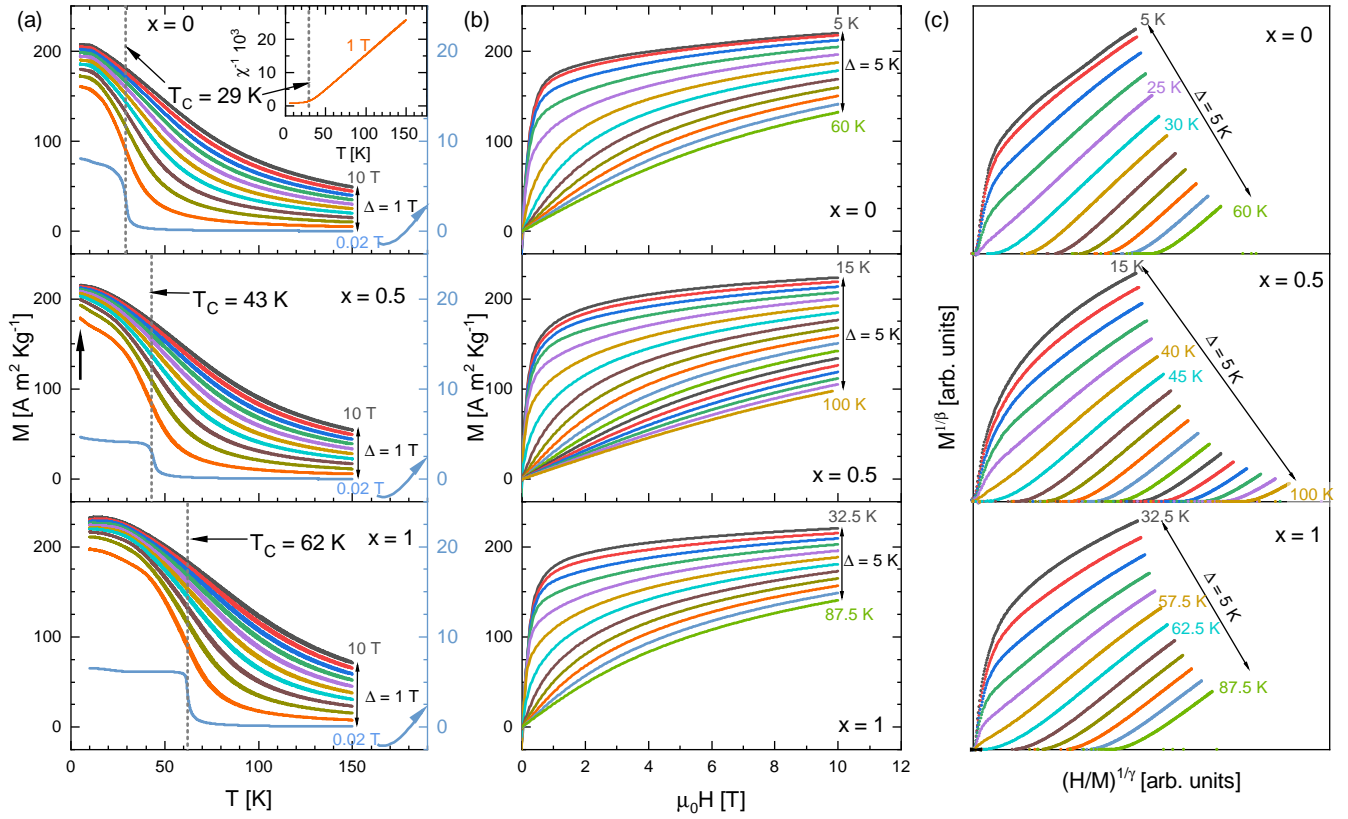


FIG. 3. Temperature (a) and field (b) dependences of the magnetization of $\text{Ho}_{1-x}\text{Dy}_x\text{Al}_2$ with $x = 0$, $x = 0.5$, and $x = 1$, respectively. Dashed lines in (a) show the position of the Curie temperatures, which were determined from the maximum in the first derivative of $M(T)$ of 0.02 T (blue lines with corresponding right y axis). For HoAl_2 in (a), the inverse magnetic susceptibility at 1 T is presented in the insert. The black arrow in (a) for $x = 0.5$ indicates an additional rise in magnetization below 10 K, which is associated to the spin-reorientation transition [36]. The corresponding modified Arrott plots, constructed from measured magnetization data, are presented in (c) for the 3D-Ising model with the critical exponents $\beta = 0.3265$ and $\gamma = 1.237$.

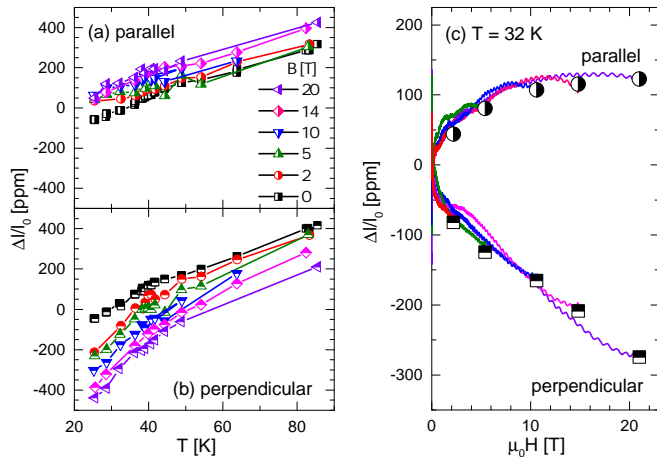


FIG. 4. Maximum values obtained for the parallel (a) and perpendicular (b) component of the relative length changes $\Delta l/l_0$ for $\text{Ho}_{0.5}\text{Dy}_{0.5}\text{Al}_2$ at various to the applied magnetic fields as function of the initial temperature. (c) Magnetic-field dependence of $\Delta l/l_0$ for different magnetic-field pulses at an initial temperature of 32 K.

sample with $x = 0$, 0.13 for $x = 0.5$, and 0.21 for $x = 1$ respectively.

With this correction, modified Arrott plots are constructed and shown in Fig. 3(c). These reflect the dependences of $M^{1/\beta}$ as function of $(H_i/M)^{1/\gamma}$, with the critical exponents β and γ . With properly chosen β and γ , the isothermal curves should be parallel with respect to each other for a well-defined second-order phase transition [57]. The best results were obtained assuming the universality class of 3D-Ising spins. However, at low temperatures, deviations from parallelism occur due to the influence of secondary phases at the spin-reorientation transitions. According to [37], the exchange interaction in RAl_2 is anisotropic due to the CEF effect and the non-spherical form of the $4f$ shells of the rare-earth atoms. Moreover, it leads to a subtle cubic to tetragonal lattice deformation around the Curie temperature [37, 43]. Recently, Murtaza *et al.* [58] studied the similar Laves-phase material NdCo_2 with ferromagnetically ordered Nd and Co magnetic sublattices, where a temperature-induced symmetry reduction from cubic $Fd\bar{3}m$ to tetragonal $I4_1/amd$ at the magnetic phase transition was observed in neutron diffraction. The authors also derived critical exponents using modified Arrott plots, the Kouvel-Fisher method, and critical-isotherm analysis and concluded, that the

resulting values correspond to the 3D-Ising model.

Furthermore, we observe an anisotropic length change $\Delta l/l_0$ in $\text{Ho}_{0.5}\text{Dy}_{0.5}\text{Al}_2$ from magnetostriction data parallel and perpendicular to the applied pulsed fields relatively to l_0 at 32 K in zero field (Fig. 4). The parallel component of $\Delta l/l_0$ increases with field and achieves a value of 120 ppm in 20 T at 32 K. At the same time, the perpendicular magnetostriction is negative and linearly decreases down to -300 ppm in 20 T. This indicates the presence of a symmetry reduction from cubic to tetragonal, as it was observed for NdCo_2 , and supports the hypothesis of a 3D-Ising-like behavior.

Specific heat C data are presented in Fig. 5. The data measured in the absence of magnetic field (black squares) shows a lambda-like anomaly around the transition temperatures. The application of external magnetic fields suppresses the phase transition. Such behaviour is typical for materials with a second-order phase transition, as visible as well in the $M(T)$ curves [Fig. 3(a)]. Below T_C , additional anomalies are observed for all three samples, which are associated with the mentioned spin-reorientation transition (T_{SR}) [36]. For HoAl_2 , there are two kinks occurring below 20 K for zero field. The anomaly around 15 K, we relate to the spin-reorientation transition [Fig. 5(a), black arrow] [36, 44]. The anomaly around 9 K, (Fig. 5(a), violet arrow) can be related to the Néel temperature (T_N) in HoAl_3 [59]. For $\text{Ho}_{0.5}\text{Dy}_{0.5}\text{Al}_2$ $T_{SR} \approx 5$ K, as shown in the inset of Fig. 5(b). This agrees well with results reported in Ref. [36]. In the case of DyAl_2 , we find no clear anomaly in zero field, but at 5 T a kink appears below 30 K [Fig. 5(c), black arrow]. The reported value in zero field is $T_{SR} \approx 40$ K [36, 44, 45].

From the specific heat data, we determined the total entropies of the magnetic material under constant applied field using the thermodynamic equation [60]:

$$S(H, T) - S_0 = \int_{T_0}^T \frac{C(H, T)}{T} dT, \quad (3)$$

where S_0 is a constant entropy at $T_0 = 2$ K. The resulting $S - T$ diagrams are shown in Figs. 5(d)-5(f). From these diagrams it is possible to calculate the isothermal entropy changes, $\Delta S_T = S(H_0, T) - S(H_1, T)$, in a magnetic field change $\Delta H = H_1 - H_0$ as the vertical distance between the $S(H_0)$ and $S(H_1)$ curves at constant temperature [orange arrow in Fig. 5(d)]. In a similar way, the adiabatic temperature changes, ΔT_{ad} , are obtained from the horizontal difference between the $S(H)$ curves.

On the other hand, ΔS_T can also be determined from magnetization measurements using the Maxwell relation [61]:

$$\Delta S_T(T, \Delta H) = \int_{H_0}^{H_1} \frac{\partial M(H, T)}{\partial T} dH. \quad (4)$$

In Figs. 6(a)-6(c), the calculated ΔS_T from specific heat is plotted as solid lines, together with the values calculated from magnetization (data points). Figures 6(d)-6(f) show the ΔT_{ad} results calculated from specific heat (lines) in comparison with the values measured directly in pulsed fields up to 50 T (symbols). There is excellent agreement between the results obtained from specific heat and magnetization. Furthermore, also the ΔT_{ad} values extracted from the $S - T$ diagrams

TABLE I. Maximum values of ΔS_T and ΔT_{ad} in $\text{Ho}_{1-x}\text{Dy}_x\text{Al}_2$, with $x = 0, 0.5, \text{ and } 1$, obtained for field changes from 0 to 5 T. Results from the present work (PW), calculated from specific heat data, are provided in comparison with literature data from references [43–45, 50–52, 62].

Sample	T_C (K)	ΔS_T ($\text{J} \cdot \text{kg}^{-1} \text{K}^{-1}$)	ΔT_{ad} (K)	Ref.
HoAl_2	29	-21.5	8.6	PW
	32	-25.1	-	[43]
	32	-27.4	-	[44]
	29	-19.6	-	[50]
	32	-25.1	-	[51]
	29.9	-28.8	-	[52]
$\text{Ho}_{0.5}\text{Dy}_{0.5}\text{Al}_2$	43	-18.8	6.8	PW
	45	-21.6	-	[52]
DyAl_2	62	-16.6	6.2	PW
	58	-18.0	-	[45]
	60	-18.5	-	[51]
	59.1	-18.5	-	[52]
	60	-17.1	-	[62]

are very close to the directly measured adiabatic temperature changes in pulsed magnetic fields. The positions of the maxima in ΔS_T and ΔT_{ad} are located close to T_C , as expected for second-order phase transitions.

In the case of HoAl_2 and DyAl_2 , the $\Delta S_T(T)$ and $\Delta T_{ad}(T)$ curves, calculated from the $S - T$ diagrams, show shoulders below T_C [see Figs. 6(a), 6(c), 6(d) and 6(f)]. In the case of $\text{Ho}_{0.5}\text{Dy}_{0.5}\text{Al}_2$, additional peaks are present, marked in Fig. 6(b) and 6(e) with black arrows. These anomalies are associated with the spin-reorientation transitions.

As mentioned, T_C increases with Dy concentration and, therefore, also the temperature of the maximum MCE shifts with x . However, the magnitude of the MCE decreases with x , at least for fields up to 20 T. This effect can be explained by considering Eq. (4). According to the Maxwell relation, the entropy change is proportional to the derivative $\partial M/\partial T$, which is largest for the alloy with the lowest Curie temperature. Interestingly, for fields of 40 and 50 T, this trend changes and $\text{Ho}_{0.5}\text{Dy}_{0.5}\text{Al}_2$ shows the largest ΔT_{ad} : 26.9 K and 30.7 K, respectively. For HoAl_2 , these values are 26.1 K at 40 T and 27.6 K at 50 T, for DyAl_2 23.6 K, and 27.8 K, respectively (Fig. 6).

Table I gives a summary about the maximum values of ΔS_T and ΔT_{ad} for field changes from 0 to 5 T for all three samples at T_C , together with reported data for comparison [43–45, 50–52, 62]. There is some scatter in the Curie temperatures and also in the size of the effect when considering the literature data. That could be related to different material syntheses and heat treatments or difference between poly- and single-crystalline samples.

Permanent magnets are typically used as the field sources for magnetic cooling devices for domestic purposes. However, when it comes to a large-scale production plant for liquid hydrogen, superconducting magnets can make perfect sense. In Fig. 7, the temperature dependencies of ΔS_T and ΔT_{ad} for 10 T field for the three samples are shown. These data nicely

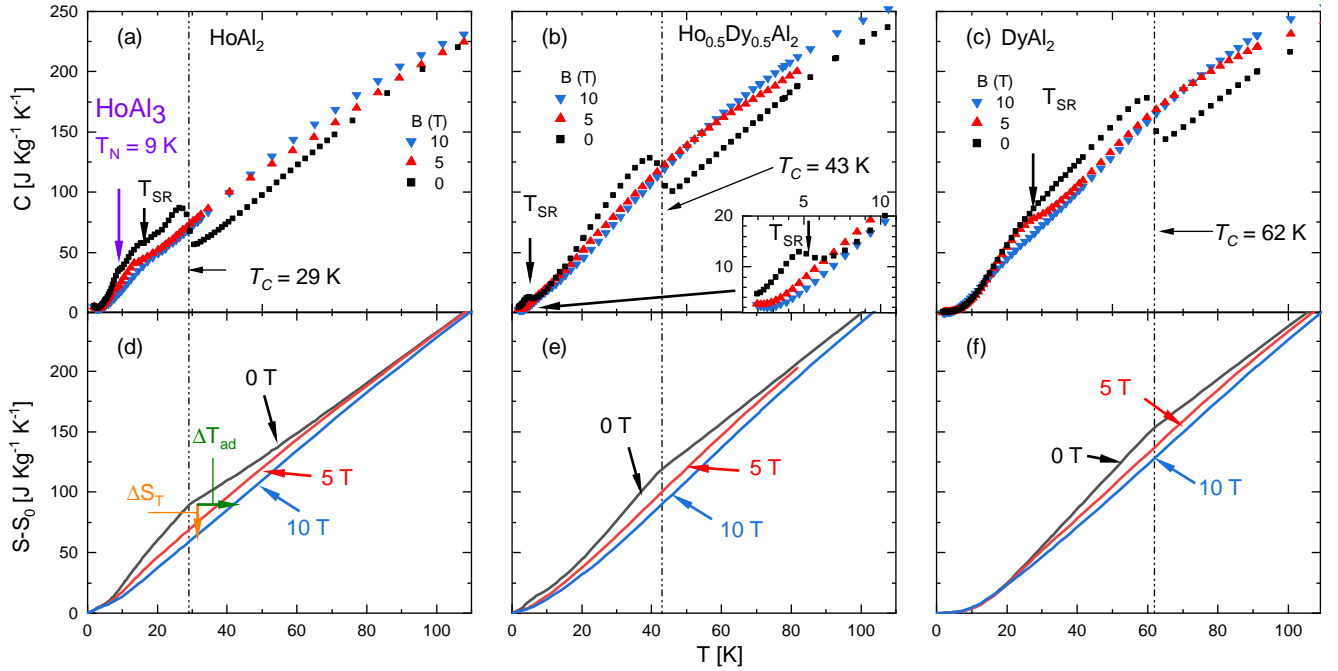


FIG. 5. Specific heat data for $\text{Ho}_{1-x}\text{Dy}_x\text{Al}_2$ (a) for $x = 0$, (b) for $x = 0.5$, and (c) for $x = 1$ measured in zero field, 5, and 10 T. Black arrows indicate the temperature-induced spin-reorientation transition. The violet arrow in (a) shows T_N for the HoAl_3 impurity phase in the HoAl_2 sample. (d-f) Calculated total entropy as function of temperature determined from the specific heat data for the samples with $x = 0, 0.5$, and 1 , respectively. In (d), the orange vertical and green horizontal arrows between the entropy curves correspond to isothermal entropy and adiabatic temperature changes for a field change of 10 T.

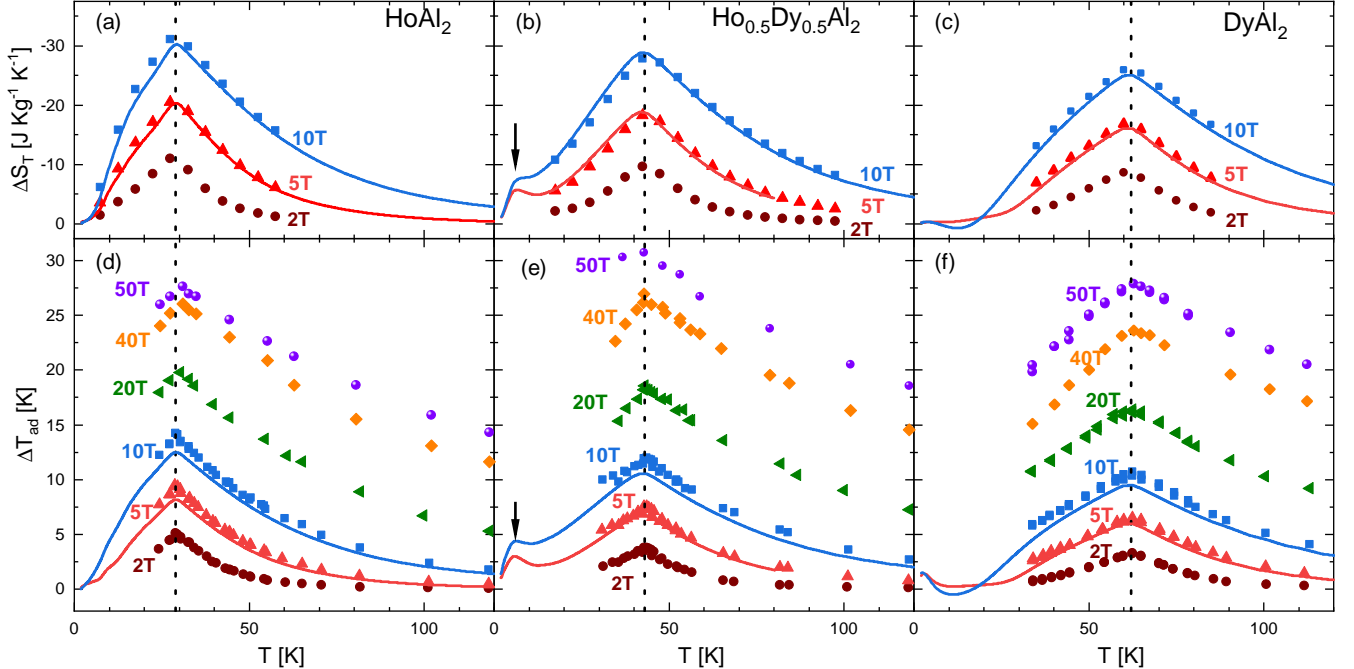


FIG. 6. Isothermal entropy changes calculated from magnetization (symbols) and specific heat (lines) as a function of temperature for $\text{Ho}_{1-x}\text{Dy}_x\text{Al}_2$ with $x = 0$ (a), $x = 0.5$ (b), and $x = 1$ (c) for magnetic field changes of 2, 5, and 10 T. Adiabatic temperature changes measured directly in pulsed fields up to 50 T (symbols) are shown in (d), (e), and (f), together with the values calculated from the specific-heat data (lines). Black arrows in (b) and (e) show separated ΔS_T and ΔT_{ad} peaks associated with spin-reorientation transition for $\text{Ho}_{0.5}\text{Dy}_{0.5}\text{Al}_2$ at $T_{\text{SR}} \approx 5$ K.

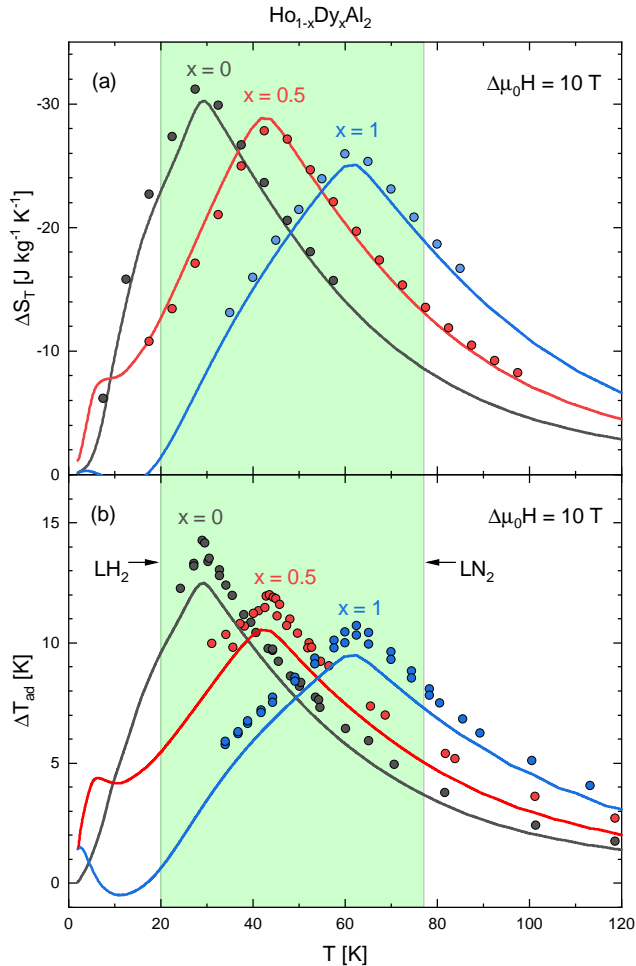


FIG. 7. ΔS_T (a) and ΔT_{ad} (b) for magnetic field changes from 0 to 10 T for $\text{Ho}_{1-x}\text{Dy}_x\text{Al}_2$, with $x = 0, 0.5,$ and 1 . Solid lines correspond to values calculated from specific heat and symbols to ΔS_T calculated from magnetization data (a) and ΔT_{ad} measured directly (b). The green area indicates the temperature window between the boiling points of liquid hydrogen at 20 K and liquid nitrogen at 77 K.

demonstrate that the MCE in the three samples covers the

whole temperature range from 77 down to 20 K as required for the last stages of magnetic hydrogen liquefaction.

IV. CONCLUSION

In this work, we provide a comprehensive experimental MCE study of $\text{Ho}_{1-x}\text{Dy}_x\text{Al}_2$ compounds with $x = 0, 0.5,$ and 1 . From X-ray powder diffraction and energy-dispersive X-ray spectroscopy data analyses we could show that all three samples were synthesized in the target Laves phase with some amount of impurities. The variation of the dysprosium-to-holmium ratio allows tuning of T_C in a broad temperature range. Our magnetization data suggest that the 3D-Ising model is the most reasonable to describe the magnetic properties in the alloys. Measurements of the magnetic field-induced $\Delta l/l_0$ in pulsed fields confirm the tetragonal distortion of the lattice and the corresponding symmetry reduction, which is another argument for interacting 3D-Ising spins. From our specific heat data, we found anomalies at the spin-reorientation transitions. Especially for $\text{Ho}_{0.5}\text{Dy}_{0.5}\text{Al}_2$, where $T_{SR} \approx 5$ K this transition is clearly separated from T_C . $\Delta S_T(T)$ was calculated from both magnetization and specific heat data, when $\Delta T_{ad}(T)$ was derived from $C(T)$ which fits very good to experimental data measured directly in pulsed magnetic fields. This work shows that the $\text{Ho}_{1-x}\text{Dy}_x\text{Al}_2$ system is very promising for magnetic H_2 liquefaction.

ACKNOWLEDGMENTS

The authors gratefully acknowledge the financial support by the Russian Science Foundation (Project No. 18-42-06201), by the HLD at HZDR, member of the European Magnetic Field Laboratory (EMFL), and the Helmholtz Association via the Helmholtz-RSF Joint Research Group (Project No. HRSF-0045). We further acknowledge support from the Deutsche Forschungsgemeinschaft (DFG, German Research Foundation) - Project-ID 405553726-TRR 270, GO 3343/2-1, SFB 1143 (Project No. 247310070), and the Würzburg-Dresden Cluster of Excellence on Complexity and Topology in Quantum Matter-*ct.qmat* (EXC 2147, Project No. 390858490).

-
- [1] Z. Navas-Anguita, D. García-Gusano, and D. Iribarren, *A review of techno-economic data for road transportation fuels*, *Renew. Sustain. Energy Rev.* **112**, 11 (2019).
 - [2] J. Lindorfer, D. C. Rosenfeld, and H. Böhm, in *Future Energy: Improved, Sustainable and Clean Options for Our Planet*, edited by T. M. Letcher (Elsevier, 2020) 3rd ed., pp. 495–517.
 - [3] K. T. Møller, T. R. Jensen, E. Akiba, and H. wen Li, *Hydrogen - A sustainable energy carrier*, *Prog. Mater. Sci.* **27**, 34 (2017).
 - [4] P. Edwards, V. Kuznetsov, W. David, and N. Brandon, *Hydrogen and fuel cells: Towards a sustainable energy future*, *Energy Policy* **36**, 4356 (2008).
 - [5] E. Tzimas, C. Filiou, S. Peteves, and J. Veyret, *Hydrogen storage: state-of-the-art and future perspective*, *EU Commission, JRC Petten, EUR 20995EN* (2003).
 - [6] G. W. Crabtree, M. S. Dresselhaus, and M. V. Buchanan, *The Hydrogen Economy*, *Phys. Today* **57**, 39 (2004).
 - [7] E. Brück, *Developments in magnetocaloric refrigeration*, *J. Phys. D: Appl. Phys.* **38**, R381 (2005).
 - [8] O. Gutfleisch, M. A. Willard, E. Brück, C. H. Chen, J. P. Sankar, and S. G. Liu, *Magnetic materials and devices for the 21st century: stronger, lighter, and more energy efficient*, *Adv. Mater.* **23**, 821 (2011).

- [9] A. Kitanovski, *Energy applications of magnetocaloric materials*, *Adv. Energy Mater.* **10**, 1903741 (2020).
- [10] J. Lyubina, *Magnetocaloric materials for energy efficient cooling*, *J. Phys. D: Appl. Phys.* **50**, 053002 (2017).
- [11] T. Gottschall, K. P. Skokov, M. Fries, A. Taubel, I. Radulov, F. Scheibel, D. Benke, S. Riegg, and O. Gutfleisch, *Making a cool choice: The materials library of magnetic refrigeration*, *Adv. Energy Mater.* **9**, 1901322 (2019).
- [12] J. A. Jensen and A. R. Mackintosh, in *Rare earth magnetism: structures and excitations*, edited by J. Birman, S. F. Edwards, C. H. Llewellyn Smith, and M. Rees (Clarendon Press, Oxford, 1991).
- [13] G. V. Brown, *Magnetic heat pumping near room temperature*, *J. Appl. Phys.* **47**, 3673 (1976).
- [14] S. A. Nikitin, E. V. Talalaeva, L. A. Chernikova, G. E. Chuprikov, T. I. Ivanova, G. V. Kazakov, and G. A. Yarkho, *Features of the magnetic behavior and of the magnetocaloric effect in a single crystal of gadolinium*, *J. Exp. Theor. Phys.* **47**, 107 (1978).
- [15] T. Hashimoto, T. Numasawa, M. Shino, and T. Okada, *Magnetic refrigeration in the temperature range from 10 K to room temperature: the ferromagnetic refrigerants*, *Cryogenics* **21**, 647 (1981).
- [16] S. Y. Dan'kov, T. I. Ivanova, and A. M. Tishin, *Thermodynamic properties of gadolinium in the vicinity of Curie point*, *Pisma JTP* **18**, 35 (1992).
- [17] T. Gottschall, M. D. Kuz'min, K. P. Skokov, Y. Skourski, M. Fries, O. Gutfleisch, M. G. Zavareh, D. L. Schlager, Y. Mudryk, V. Pecharsky, and J. Wosnitzer, *Magnetocaloric effect of gadolinium in high magnetic fields*, *Phys. Rev. B* **99**, 134429 (2019).
- [18] C. Wu, Z. Yu, K. Sun, J. Nie, R. Guo, H. Liu, X. Jiang, and Z. Lan, *Calculation of exchange integrals and Curie temperature for La-substituted barium hexaferrites*, *Sci. Rep.* **6**, 36200 (2016).
- [19] L. Morellon, Z. Arnold, C. Magen, C. Ritter, O. Prokhnenko, Y. Skorokhod, P. A. Algarabel, M. R. Ibarra, and J. Kamarad, *Pressure Enhancement of the Giant Magnetocaloric Effect in $Tb_5Si_2Ge_2$* , *Phys. Rev. Lett.* **93**, 137201 (2004).
- [20] A. M. G. Carvalho, C. S. Alves, A. de Campos, A. A. Coelho, S. Gama, F. C. Gandra, P. J. von Ranke, and N. A. Oliveira, *The magnetic and magnetocaloric properties of $Gd_5Ge_2Si_2$ compound under hydrostatic pressure*, *J. Appl. Phys.* **97**, 10M320 (2005).
- [21] T. Gottschall, E. Bykov, A. Gràcia-Condal, B. Beckmann, A. Taubel, L. Pfeuffer, O. Gutfleisch, L. Mañosa, A. Planes, Y. Skourski, and J. Wosnitzer, *Advanced characterization of multicaloric materials in pulsed magnetic fields*, *J. Appl. Phys.* **127**, 185107 (2020).
- [22] D. Yu. Karpenkov, A. Yu. Karpenkov, K. P. Skokov, I. A. Radulov, M. Zheleznyi, T. Faske, and O. Gutfleisch, *Pressure Dependence of Magnetic Properties in $La(Fe,Si)_{13}$: Multistimulus Responsiveness of Caloric Effects by Modeling and Experiment*, *Phys. Rev. Appl.* **13**, 034014 (2020).
- [23] Z. B. Guo, Y. W. Du, J. S. Zhu, H. Huang, W. P. Ding, and D. Feng, *Large magnetic entropy change in perovskite-type manganese oxides*, *Phys. Rev. Lett.* **78**, 1142 (1997).
- [24] H. Wada and Y. Tanabe, *Giant magnetocaloric effect of $MnAs_{1-x}Sb_x$* , *Appl. Phys. Lett.* **79**, 3302 (2001).
- [25] H. Zhang, Y. J. Sun, E. Niu, L. H. Yang, J. Shen, F. X. Hu, J. R. Sun, and B. G. Shen, *Large magnetocaloric effects of $RFeSi$ ($R = Tb$ and Dy) compounds for magnetic refrigeration in nitrogen and natural gas liquefaction*, *Appl. Phys. Lett.* **103**, 202412 (2013).
- [26] M. Krautz, K. Skokov, T. Gottschall, C. S. Teixeira, A. Waske, J. Liu, L. Schultz, and O. Gutfleisch, *Systematic investigation of Mn substituted $La(Fe,Si)_{13}$ alloys and their hydrides for room-temperature magnetocaloric application*, *J. Alloys Compd.* **598**, 27 (2014).
- [27] A. Taubel, T. Gottschall, M. Fries, T. Faske, K. P. Skokov, and O. Gutfleisch, *Influence of magnetic field, chemical pressure and hydrostatic pressure on the structural and magnetocaloric properties of the Mn-Ni-Ge system*, *J. Phys. D: Appl. Phys.* **50**, 464005 (2017).
- [28] A. Davarpanah, I. Radulov, N. Shayanfar, F. Maccari, K. Skokov, J. Amaral, and O. Gutfleisch, *The impact of Pr and Nd substitution on structure, hysteresis and magnetocaloric properties of $La_{1-x}(Pr,Nd)_xFe_{11.6}Si_{1.4}$* , *J. Phys. D: Appl. Phys.* **54**, 225001 (2021).
- [29] F. Stein, M. Palm, and G. Sauthoff, *Structure and stability of Laves phases. Part I. Critical assessment of factors controlling Laves phase stability*, *Intermetallics* **12**, 713 (2004).
- [30] W. R. Johanson, G. Pierce, C. B. Zimm, and J. A. Barclay, *Heat capacity of $Gd_{0.06}Er_{0.94}Al_2$ in magnetic fields*, *J. Appl. Phys.* **64**, 5892 (1988).
- [31] K. A. Gschneidner, V. K. Pecharsky, and S. K. Malik, in *Advances in Cryogenic Engineering Materials*, Vol. 42, edited by L. T. Summers (Springer, Boston, MA, 1996) pp. 475–483.
- [32] K. A. Gschneidner, V. K. Pecharsky, M. J. Gailloux, and H. Takeya, in *Advances in Cryogenic Engineering Materials*, Vol. 42, edited by L. T. Summers (Springer, Boston, MA, 1996) pp. 465–474.
- [33] F. W. Wang, X. X. Zhang, and F. X. Hu, *Large magnetic entropy change in $TbAl_2$ and $(Tb_{0.4}Gd_{0.6})Al_2$* , *Appl. Phys. Lett.* **77**, 1360 (2000).
- [34] D. Wang, H. Liu, S. Tang, S. Yang, S. Huang, and Y. Du, *Magnetic properties and magnetocaloric effects in $(Gd_xDy_{1-x})Co_2$ compounds*, *Phys. Lett. A* **297**, 247 (2002).
- [35] N. A. de Oliveira and P. J. von Ranke, *Magnetocaloric effect in the Laves phase pseudobinaries $(Dy_{1-c}R_c)Al_2$ ($R = Er$ and Ho)*, *J. Magn. Magn. Mater.* **320**, 386 (2008).
- [36] M. Khan, K. A. Gschneidner Jr, and V. K. Pecharsky, *Spin reorientation transitions in $Ho_{1-x}Dy_xAl_2$ alloys*, *J. Appl. Phys.* **110**, 103912 (2011).
- [37] H. G. Purwins and A. Leson, *Magnetic properties of (rare earth) Al_2 intermetallic compounds*, *Adv. Phys.* **39**, 309 (1990).
- [38] P. J. von Ranke, N. A. de Oliveira, D. C. Garcia, V. S. R. de Sousa, V. A. de Souza, A. M. G. Carvalho, S. Gama, and M. S. Reis, *Magnetocaloric effect due to spin reorientation in the crystalline electrical field: Theory applied to $DyAl_2$* , *Phys. Rev. B* **75**, 184420 (2007).
- [39] M. Kim, N. Sung, Y. Son, M. Ko, and B. Cho, *Giant reversible anisotropic magnetocaloric effect in an antiferromagnetic $EuFe_2As_2$ single crystal*, *Appl. Phys. Lett.* **98**, 172509 (2011).
- [40] M. Fries, K. P. Skokov, D. Y. Karpenkov, V. Franco, S. Ener, and O. Gutfleisch, *The influence of magnetocrystalline anisotropy on the magnetocaloric effect: A case study on Co_2B* , *Appl. Phys. Lett.* **109**, 232406 (2016).
- [41] B. Daudin and E. Bonjour, *Specific-heat of $HoAl_2$ with external magnetic-field*, *C. R. Seances Acad. Sci. Ser. II (France)* **295**, 535 (1982).
- [42] I. G. de Oliveira, D. C. Garcia, and P. J. von Ranke, *Spin reorientation and magnetocaloric effect study in $HoAl_2$ by a microscopic model Hamiltonian*, *J. Appl. Phys.* **102**, 073907 (2007).
- [43] L. A. Gil, J. C. P. Campoy, E. J. R. Plaza, and M. V. de Souza, *Conventional and anisotropic magnetic entropy change in $HoAl_2$ ferromagnetic compound*, *J. Magn. Magn. Mater.* **409**,

- 45 (2016).
- [44] J. C. B. Monteiro and F. G. Gandra, *Direct measurements of conventional and anisotropic magnetocaloric effect in binary RA_2 single crystals*, *J. Appl. Phys.* **121**, 213904 (2017).
- [45] A. L. Lima, A. O. Tsokol, K. A. Gschneidner Jr, V. K. Pecharsky, T. A. Lograsso, and D. L. Schlagel, *Magnetic properties of single-crystal $DyAl_2$* , *Phys. Rev. B* **72**, 024403 (2005).
- [46] S. Taskaev, V. Khovaylo, K. Skokov, W. Liu, E. Bykov, M. Ulyanov, D. Bataev, A. Basharova, M. Kononova, D. Iakhot-skiy, M. Bogush, M. Gavrilova, T. Gottschall, and Z. Hu, *Magnetocaloric effect in polycrystalline $DyAl_2$* , *Chelyabinsk Physical and Mathematical Journal* **5**, 618 (2020).
- [47] J. Rodríguez-Carvajal, *Recent advances in magnetic structure determination by neutron powder diffraction*, *Physica B Condens. Matter* **192**, 55 (1993).
- [48] L. Pfeuffer, T. Gottschall, T. Faske, A. Taubel, F. Scheibel, A. Y. Karpenkov, S. Ener, K. P. Skokov, and O. Gutfleisch, *Influence of the martensitic transformation kinetics on the magnetocaloric effect in $Ni-Mn-In$* , *Phys. Rev. Materials* **4**, 111401(R) (2020).
- [49] A. Kitanovski, J. Tušek, U. Tomc, U. Plaznik, M. Ožbolt and A. Poredoš, in *Magnetocaloric energy conversion: From theory to applications*. (Springer, Switzerland, 2015).
- [50] S. Baran, R. Duraj, and A. Szytuła, *Magnetocaloric effect and transition order in $HoAl_2$* , *Acta Phys. Pol. A* **127**(3), (2015).
- [51] J. C. P. Campoy, E. J. R. Plaza, A. A. Coelho, and S. Gama, *Magnetoresistivity as a probe to the field-induced change of magnetic entropy in RA_2 compounds ($R = Pr, Nd, Tb, Dy, Ho, Er$)*, *Phys. Rev. B* **74**, 134410 (2006).
- [52] T. Hashimoto, T. Kuzuhara, M. Sahashi, K. Inomata, A. Tomokiyo, and H. Yayama, *New application of complex magnetic materials to the magnetic refrigerant in an Ericsson magnetic refrigerator*, *J. Appl. Phys.* **62**, 3873 (1987).
- [53] M. Patra, S. Majumdar, S. Giri, Y. Xiao, and T. Chatterji, *Magnetic, magnetocaloric and magnetoresistive properties of cubic Laves phase $HoAl_2$ single crystal*, *J. Phys.: Condens. Matter* **26**, 046004 (2014).
- [54] B. Leon, V. U. S. Rao, and W. E. Wallace, *Magnetic characteristics of the aluminum-rich ternary laves phases containing rare earths, nickel and aluminum*, *J. Less Common Met.* **24**, 247 (1971).
- [55] A. Chelkowski, E. Talik, and G. Wnętrzak, *Magnetic susceptibility and electric resistivity investigation in $Gd_{1-x}Dy_xAl_2$* , *Solid State Commun.* **46**, 759 (1983).
- [56] R. C. O'handley, in *Modern magnetic materials: principles and applications*. (Wiley, New York, 2000).
- [57] A. Arrott and J. E. Noakes, *Approximate equation of state for nickel near its critical temperature*, *Phys. Rev. Lett.* **19**, 786 (1967).
- [58] A. Murtaza, W. Zuo, J. Mi, Y. Li, A. Ghani, M. Yaseen, M. T. Khan, C. Hao, K. Li, Z. Dai, S. Yang, and Y. Ren, *Magnetocaloric effect and critical exponent analysis around magnetic phase transition in $NdCo_2$ compound*, *J. Phys. D: Appl. Phys.* **53**, 345003 (2020).
- [59] A. Chelkowski, Table 1, part 2; Table 2. in *Compounds of Rare Earth Elements with Main Group Elements. Part 2*, Vol. 19E2, edited by H. P. J. Wijn (Springer-Verlag Berlin Heidelberg, 1989) pp. 163–175. <https://materials.springer.com>.
- [60] A. M. Tishin and Y. I. Spichkin, in *The magnetocaloric effect and its applications*. (CRC Press, 2016).
- [61] V. Franco, J. Blázquez, J. Ipus, J. Law, L. Moreno-Ramírez, and A. Conde, *Magnetocaloric effect: From materials research to refrigeration devices*, *Prog. Mater. Sci.* **93**, 112 (2018).
- [62] V. Pecharsky and K. Gschneidner, in *Advances in Cryogenic Engineering Materials*, Vol. 42, edited by L. T. Summers (Springer, Boston, MA, 1996) pp. 423–430.